The Astrophysical Journal, 845:166 (5pp), 2017 August 20 https://doi.org/10.3847/1538-4357/aa8308

Prospects of Dynamical Determination of General Relativity Parameter β and Solar Quadrupole Moment $J_{2\odot}$ with Asteroid Radar Astronomy

Ashok K. Verma[1], Jean-Luc Margot[1,2], and Adam H. Greenberg[2]
[1] Department of Earth, Planetary, and Space Sciences, University of California, Los Angeles, CA 90095, USA; ashokverma@ucla.edu
[2] Department of Physics and Astronomy, University of California, Los Angeles, CA 90095, USA
Received 2017 May 29; revised 2017 July 25; accepted 2017 July 26; published 2017 August 23

Abstract

We evaluated the prospects of quantifying the parameterized post-Newtonian parameter β and solar quadrupole moment $J_{2\odot}$ with observations of near-Earth asteroids with large orbital precession rates (9 to 27 arcsec century^{-1}). We considered existing optical and radar astrometry, as well as radar astrometry that can realistically be obtained with the Arecibo planetary radar in the next five years. Our sensitivity calculations relied on a traditional covariance analysis and Monte Carlo simulations. We found that independent estimates of β and $J_{2\odot}$ can be obtained with precisions of 6×10^{-4} and 3×10^{-8}, respectively. Because we assumed rather conservative observational uncertainties, as is the usual practice when reporting radar astrometry, it is likely that the actual precision will be closer to 2×10^{-4} and 10^{-8}, respectively. A purely dynamical determination of solar oblateness with asteroid radar astronomy may therefore rival the helioseismology determination.

Key words: astrometry – gravitation – minor planets, asteroids: general – relativistic processes – Sun: fundamental parameters – techniques: radar astronomy

1. Introduction

The parameterized post-Newtonian (PPN) formalism is a useful framework for testing metric theories of gravity (Will 2014). It consists of 10 dimensionless parameters that describe the general properties of the metric. In general relativity (GR), only 2 of the 10 parameters are non-zero. They are known as the Eddington–Robertson–Schiff parameters γ and β. γ represents the amount of curvature produced by a unit mass, and β represents the amount of nonlinearity in the superposition law for gravity.

Several techniques have been used to place observational bounds on these parameters (Will 2014), including observations of the bending and delay of light by spacecraft tracking (e.g., Bertotti et al. 2003) or Very Long Baseline Interferometry (e.g., Lambert & Le Poncin-Lafitte 2009), and fitting of ephemerides to observations of planetary positions (e.g., Folkner 2009; Fienga et al. 2011; Verma et al. 2014; Fienga et al. 2015).

In GR, γ and β are equal to one. Doppler tracking of the *Cassini* spacecraft has shown that γ does not differ from one by more than 2×10^{-5} (Bertotti et al. 2003). Ephemeris-based studies prior to 2009 indicated that $\beta - 1$ does not differ from zero by more than 10^{-4} (Folkner 2009; Pitjeva & Pitjev 2014). More recently, the availability of precise ranging data from the MESSENGER Mercury orbiter (Solomon et al. 2001) enabled improved estimates (Verma et al. 2014; Fienga et al. 2015; Park et al. 2017). Here, we evaluate the prospect of asteroid orbit precession measurements to place more stringent bounds on β. We consider Earth-based radar observations of near-Earth asteroids with perihelion shifts larger than 10 arcsec century^{-1}.

Orbital precession can also be caused by the nonuniformity of the gravity field that results from the oblate shape of the Sun. The solar oblateness is characterized by the solar quadrupole moment, $J_{2\odot}$ (e.g., Kaula 2000). Simultaneous estimation of β and $J_{2\odot}$ requires that the precessional effects due to GR and to the Sun's oblateness be disentangled. Fortunately, GR is a purely central effect, whereas the oblateness-induced precession has an inclination dependence. The two effects also have a different distance dependence (Misner et al. 1973). As a result, observations of a small sample of near-Earth asteroids with a variety of semimajor axes and inclinations (Table 1) can in principle be used to estimate β and $J_{2\odot}$ (Margot 2003; Margot & Giorgini 2009).

Current estimates of the solar quadrupole moment are typically derived on the basis of interior models of the Sun constrained by helioseismology data (e.g., Mecheri et al. 2004; Antia et al. 2008). The current best value from the helioseismology literature is $J_{2\odot} = (2.2 \pm 0.1) \times 10^{-7}$ (Will 2014). Dynamical estimates that do not rely on fits to helioseismology data yield similar values of $J_{2\odot} = 2.3 \pm 0.25 \times 10^{-7}$ (Fienga et al. 2015) and $J_{2\odot} = 2.25 \pm 0.09 \times 10^{-7}$ (Park et al. 2017). High-precision dynamical estimates are important to validate our understanding of the interior structure of the Sun.

Our simulations of the determination of β and $J_{2\odot}$ using a variety of asteroid orbits suggest that independent values of β and $J_{2\odot}$ can be obtained with satisfactory precision: with the traditionally conservative assignment of radar uncertainties, β can be constrained at the 6×10^{-4} level and $J_{2\odot}$ can be constrained at the 3×10^{-8} level. With uncertainties that more closely reflect measurement errors, this precision may be improved by a factor of $\sim$3. (Section 4).

The outline of this paper is as follows. In Section 2, we describe our choice of target asteroids. In Section 3, we discuss the estimation of asteroid orbits with optical and radar measurements. Our dynamical model and data reduction procedures are described in Sections 3.1 and 3.2, respectively. Orbit determination results are presented in Section 3.3. Simulations of the determination of β and $J_{2\odot}$ are described in Section 4.

Table 1
Selected Asteroids and Orbital Elements: Semimajor Axis (a), Eccentricity (e), and Inclination with Respect to the Ecliptic (i_{ec}) and Sun's Equator (i_{eq})

Target	a (au)	e	i_{ec} (deg)	i_{eq} (deg)	$\dot{\delta\omega}$ ($''$ cy^{-1})
1566 Icarus	1.078	0.827	22.9	15.8	10.1
1998 TU3	0.787	0.484	5.41	3.41	9.11
1999 KW4	0.642	0.688	38.9	46.0	22.1
1999 MN	0.674	0.665	2.02	5.25	18.5
2000 BD19	0.876	0.895	25.7	28.0	26.9
2000 EE14	0.662	0.533	26.5	26.1	15.0
2001 YE4	0.677	0.541	4.82	11.0	14.4
2004 KH17	0.712	0.499	22.1	14.9	12.0
2006 CJ	0.676	0.755	10.3	16.1	23.7

Note. The predicted rate of perihelion advance in arcseconds per century ($''$ cy^{-1}), $\dot{\delta\omega}$, was computed using Equation (1).

2. Target Asteroids

The per-orbit secular advance in the angular position of the perihelion is given by (Misner et al. 1973)

$$\delta\omega = \frac{6\pi GM_\odot}{a(1-e^2)c^2}\left[\frac{(2-\beta+2\gamma)}{3}\right] + \frac{6\pi}{2}R_\odot^2\frac{(1-3/2\sin^2 i)}{a^2(1-e^2)^2}J_{2\odot}, \quad (1)$$

where ω is the argument of perihelion, $GM_\odot$ is the Sun's gravitational parameter, $R_\odot$ is the radius of the Sun, c is the speed of light, and a, e, and i are the semimajor axis, eccentricity, and orbital inclination (with respect to the solar equator) of a planetary body, respectively. Because both GR and solar oblateness affect perihelion precession, estimates of β and $J_{2\odot}$ are highly correlated and it is desirable to track a variety of solar system bodies with a range of a, e, i values to disentangle the two effects.

Our selection of target asteroids follows the method of Margot (2003). We select asteroids with both large perihelion shift values and favorable observing conditions with radar (Table 1 and Figure 1). This sample of asteroid orbits includes a wide range of semimajor axes, eccentricities, and inclinations, which are advantageous when simultaneously solving for β and $J_{2\odot}$. The predicted rates of perihelion advance, $\dot{\delta\omega}$, shown in Figure 1 and Table 1 were computed assuming $\gamma = \beta = 1$ and $J_{2\odot} = 2.2 \times 10^{-7}$.

3. Methods

We first determined nominal trajectories for asteroids in our sample with astrometric (i.e., positional) data, both optical and radar (Table 2). The process involved three steps: (1) numerical integration of each asteroid's orbit and calculation of partial derivatives of the equations of motion with respect to the solve-for parameters (i.e., the six components of the state vectors), (2) evaluation of simulated optical and radar observables and computation of their partial derivatives with respect to the solve-for parameters, and (3) least-squares adjustments to the solve-for parameters.

We used the Mission Operations and Navigation Toolkit Environment (MONTE) software (Evans et al. 2016; MONTE v124) for orbit determination and parameter estimation. MONTE is an astrodynamics computing platform developed by NASA's Jet Propulsion Laboratory (JPL). MONTE is used for spacecraft navigation and trajectory design. MONTE has also been used for a variety of scientific purposes, including gravity analysis (Verma & Margot 2016) and ephemeris generation (Greenberg et al. 2017).

3.1. Dynamical Model

MONTE uses a variable-step Adams-Bashforth method to numerically integrate the equations of motion and corresponding partial derivatives. Our dynamical model includes gravitational forces from the Sun, 8 planets, and 21 minor planets with well-determined masses (Konopliv et al. 2011), general relativistic effects, and perturbations due to the oblateness of the Sun.

In addition to these forces, we have also modeled the nongravitational Yarkovsky orbital drift. Perihelion advance due to GR and solar oblateness does not affect the value of the semimajor axis, but Yarkovsky drift does. This nongravitational effect has been shown to affect the semimajor axes of small bodies due to the anisotropic re-emission of absorbed sunlight (e.g., Bottke et al. 2006). The change in semimajor axis with time due to Yarkovsky orbital drift, $\langle da/dt\rangle$, was estimated for all target asteroids with the method of Greenberg et al. (2017). The values ranged in amplitude between 4 and 50 au/My, which is plausible for kilometer-sized bodies. Only one target (1566 Icarus) is common between our target list and the 42 Yarkovsky detections of Nugent et al. (2012), and only one target (1999 MN) is common between our target list and the 21 Yarkovsky detections of Farnocchia et al. (2013). In both cases, our Yarkovsky drift estimates are consistent with and better constrained than prior work.

To initialize the integration process, we used a priori state vectors extracted from the Minor Planet Center (MPC) database (Minor Planet Center 2017).

3.2. Existing Optical and Radar Astrometry

We used both optical and radar astrometry to determine the nominal trajectory of each asteroid. Optical measurements provide positional information on the plane of the sky. They are typically expressed as right ascension (R.A.) and declination (decl.) in the equatorial frame of epoch J2000.0. We downloaded optical astrometry from the MPC (Minor Planet Center 2017). We debiased optical astrometry and assigned data weights according to the algorithm recommended by Farnocchia et al. (2015).

Radar astrometry consists of round-trip light time, a measurement that can provide the asteroid–observer distance, and Doppler shift, a measurement that can provide the line-of-sight velocity of the asteroid with respect to the observer. Radar measurements have fractional uncertainties as small as 10^{-8}. The addition of radar astrometry can decrease orbital element uncertainties by orders of magnitude compared to an optical-only orbit solution (Ostro & Giorgini 2004). However, the number of radar measurements is typically small compared to the number of optical observations (Table 2).

We processed a total of 12,102 optical measurements (R.A. and decl. pairs obtained at 6051 epochs), as well as 56 range and 17 Doppler measurements that have been published.

3.3. Orbit Determination for Nominal Trajectories

In order to compute nominal asteroid trajectories, we computed the expected values of the observables and their

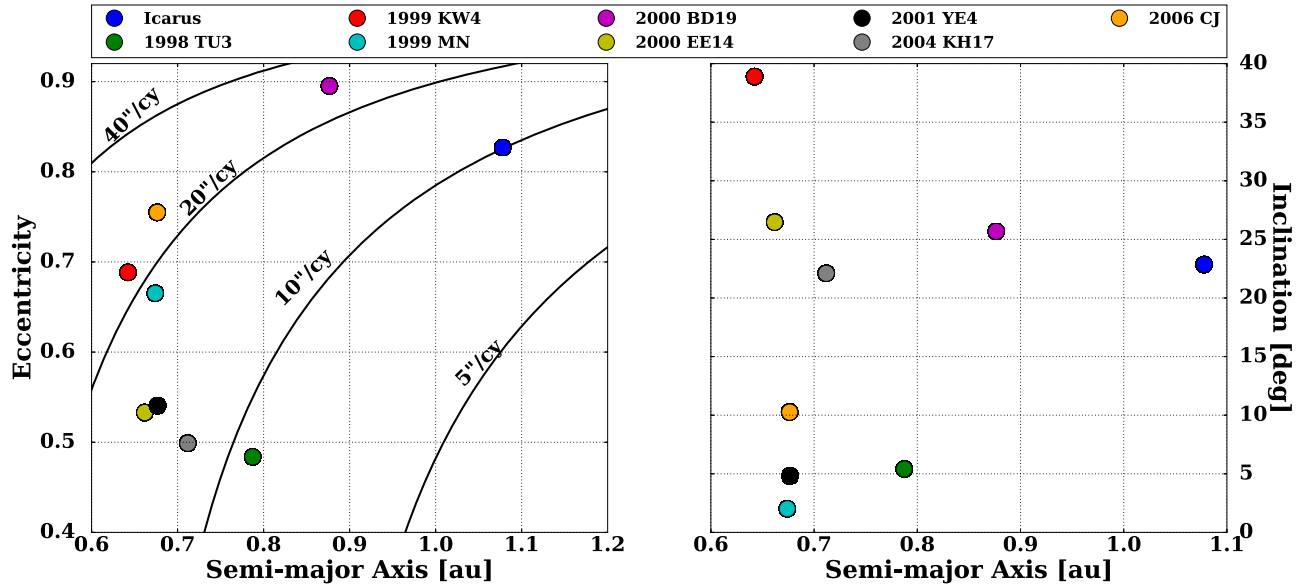

Figure 1. Distribution of asteroid orbital elements for asteroids in our sample. The corresponding rates of perihelion shift, predicted with Equation (1), are shown as contour lines.

partial derivatives with respect to initial state vectors. We calculated weighted residuals by subtracting computed measurements (C) from observed measurements (O) and dividing the result by the corresponding observational uncertainty (σ). We adjusted initial state vectors with an iterative least-squares techniques that minimized the sum of squares of weighted residuals. Because there are 9 targets and 6 orbital elements per asteroid in the nominal situation ($\gamma = 1$, $\beta = 1$, $J_{2\odot} = 2.2 \times 10^{-7}$), we adjusted a total of 54 parameters.

We defined outliers as measurements with weighted residuals in excess of three. We identified and rejected 127 epochs with outliers in the optical astrometry. There were no outliers in the radar astrometry. We obtained a measure of the quality of the fit at each iteration by computing the dimensionless rms of the weighted residuals:

$$\mathrm{rms} = \sqrt{\frac{1}{N}\sum_{i=1}^{N}\left(\frac{O_i - C_i}{\sigma_i}\right)^2}, \qquad (2)$$

where N is the number of observations, O_i is the ith observation, C_i is the ith computed measurement, and σ_i is the observational uncertainty associated with the ith observation. We stopped the iterative process when the change in the rms of the weighted residuals between two successive iterations was less than 0.01%. rms residuals smaller than one indicate solutions that provide good fits to the observations (Table 2).

3.4. Anticipated Radar Astrometry

The objectives of this study are to evaluate the precision with which PPN parameter β and solar quadrupole moment $J_{2\odot}$ can be determined from orbital fits constrained by existing and anticipated optical and radar astrometry. To quantify the effect of anticipated radar astrometry on the determination of these parameters, we simulated all existing optical and radar astrometry (Table 2) and a number of anticipated Arecibo Observatory range measurements (Table 3) with the nominal asteroid trajectories described above. We did not attempt to simulate the effect of additional optical astrometry, which is expected to improve the overall quality of the fits, albeit not as powerfully as radar astrometry (Ostro & Giorgini 2004).

To supplement the published astrometry with realistic anticipated values, we used the epochs of closest approach to Earth when the asteroids are detectable with the Arecibo radar (Table 3). On the basis of prior experience, we assumed that two to four independent data points would be collected at each future apparition. For apparitions in the past (identified in bold in Table 3), we used the number of data points that were actually obtained. In total, we simulated 61 independent range measurements in addition to the 56 published values. For each realization in our simulations, we added noise to the observations by randomly drawing from a Gaussian distribution with zero mean and standard deviation equal to the observational uncertainty. Observational uncertainties for observations in the future were assigned according to signal-to-noise ratio (S/N) and experience, with values ranging between 30 and 900 m. Uncertainties for observations in the past mirrored the actual measurement uncertainties adopted by the observer for these data points.

3.5. Orbit Determination with Estimation of β and $J_{2\odot}$

We assigned solve-for parameters to one of two categories: local and global. Local parameters are specific to each asteroid, i.e., the 6 orbital elements or initial state vector (total of $9 \times 6 = 54$ parameters), whereas global parameters are common to all asteroids, i.e., β and $J_{2\odot}$. We jointly solved for these 56 parameters.

We used two independent approaches to evaluate the precision in the determination of global parameters β and $J_{2\odot}$. First, we used a traditional covariance analysis (Section 4.1) as described in Bierman (1977). Second, we performed Monte Carlo simulations (Section 4.2) to verify the results of the covariance analysis.

4. Results

4.1. Covariance Analysis

A covariance analysis is a powerful technique that can be used to evaluate the precision of solve-for parameters. First,

Table 2
Selected Asteroids and Corresponding Observations: Observational Interval, Number of Optical Pairs (R.A. and Decl.) of Observations, and Number of Published Range and Doppler Observations

Target	Observational Interval	N_{opt}	N_{rng}	N_{dop}	rms_{opt}	rms_{rng}	rms_{dop}
1566 Icarus	1949 Jun–2015 Jul	1230	10	13	0.56	0.28	1.10
1998 TU3	1982 Dec–2016 Nov	860	⋯	⋯	0.47	⋯	⋯
2000 BD19	1997 Feb–2016 Apr	522	⋯	⋯	0.51	⋯	⋯
1999 KW4	1998 May–2016 Jul	2117	36	⋯	0.39	0.39	⋯
1999 MN	1999 Jun–2015 Jun	141	⋯	⋯	0.64	⋯	⋯
2000 EE14	2000 Mar–2016 Jun	396	⋯	⋯	0.48	⋯	⋯
2001 YE4	2001 Dec–2017 Jan	336	4	1	0.50	0.23	0.07
2004 KH17	2004 May–2016 May	211	1	⋯	0.62	0.01	⋯
2006 CJ	2006 Feb–2017 Feb	238	5	3	0.59	0.30	0.11

Note. The last three columns provide the post-fit rms of weighted residuals.

Table 3
Selected Asteroids and Simulated Observations: Years of Close Earth Approaches (yyyy − 2000), Number of Simulated Radar Ranges, and Corresponding Uncertainties

Target	Year of Close Approach	N_{range}	Uncertainties (m)
1998 TU3	**12**, 19	5	75–900
1999 KW4	**16**, 17, 18, 19, 20	12	40–300
1999 MN	**04**, **05**	2	75–600
2000 BD19	**06**, **07**, 20	10	300–375
2000 EE14	**07**, **08**, 21, 22	11	300–600
2001 YE4	**12**, **16**, 21	10	30–600
2004 KH17	**13**	2	300
2006 CJ	**12**, **17**, 22	9	60–300

Note. Years highlighted in bold correspond to epochs for which data have already been collected. The next detectable approach of 1566 Icarus is not until 2024.

simulated, noise-free measurements and their partial derivatives are computed on the basis of nominal trajectories. A least-squares estimation is then performed, where the estimates logically converge on the nominal values. In the process, the associated covariance matrix is produced. The expected precision of the estimated parameters is then inferred by examining the covariance matrix. The square roots of the diagonal elements provide the one-standard-deviation formal uncertainties.

After global fits of 56 parameters, we obtained the following formal uncertainties:

$$\sigma_\beta = 5.6 \times 10^{-4}, \quad (3)$$

$$\sigma_{J_{2\odot}} = 2.7 \times 10^{-8}, \quad (4)$$

with a correlation coefficient of −0.72. The parameters remain correlated because both GR and solar oblateness contribute to perihelion precession. However, the range of asteroid orbital parameters (Table 1) helps reduce the correlation coefficient. Consideration of the Lense-Thirring effect for the Sun increases our σ_β and $\sigma_{J_{2\odot}}$ estimates by 0.2% and 4%, respectively.

The expected formal uncertainty on $J_{2\odot}$ with direct dynamical measurement of asteroids is 2.7 times the uncertainty based on fits to helioseismology data (Antia et al. 2008). For β, the expected formal uncertainty is about twice the uncertainty obtained with pre-MESSENGER planetary ephemerides (Konopliv et al. 2011), ∼7 times the uncertainty obtained with post-MESSENGER planetary ephemerides (Verma et al. 2014; Will 2014; Fienga et al. 2015), and ∼14 times the uncertainty obtained with MESSENGER range data (Park et al. 2017). The formal uncertainties scale linearly with the uncertainties assigned to the measurements. It is often the case that radar observers assign conservative uncertainties, as evidenced by rms residuals or reduced chi-square metrics that are almost always smaller than unity and most often <0.3 (Table 2). Therefore, we anticipate that the actual precision may be improved by a factor of ∼3, and the dynamical determination of $J_{2\odot}$ may be as precise as the helioseismology determination.

In order to investigate the benefit of future observations, we also performed covariance analyses under the assumption that observations would stop at the end of 2017, 2019, or 2021, as opposed to 2022 in our nominal scenario. The results were $\sigma_{\beta,2017} = 9.6 \times 10^{-4}$, $\sigma_{\beta,2019} = 7.6 \times 10^{-4}$, $\sigma_{\beta,2021} = 7.5 \times 10^{-4}$ and $\sigma_{J_{2\odot},2017} = 1.9 \times 10^{-7}$, $\sigma_{J_{2\odot},2019} = 4.2 \times 10^{-8}$, $\sigma_{J_{2\odot},2021} = 3.8 \times 10^{-8}$.

4.2. Monte Carlo Simulations

More robust results can be obtained by performing end-to-end simulations that approximate the actual measurement and estimation process. In these analyses, integration of the trajectories and estimation of the parameters are conducted as described in Section 3 with two variations. First, we chose initial values of the solve-for parameters that are not identical to their nominal values. For instance, the initial positions and velocities of all asteroids were changed by 10 km and 0.1 m s^{-1} in each direction, respectively. Likewise, initial values for β and $J_{2\odot}$ were changed by 4×10^{-4} and 5×10^{-8}, which is approximately five times the uncertainty of recent estimates. Second, we polluted the simulated measurements with independent noise realizations as described in Section 3.

We performed 500 Monte Carlo simulations. After convergence of the least-squares estimation, we compared the estimated values of solve-for parameters with their nominal values, which produced error estimates. To arrive at an estimate of the uncertainties, we can fit Gaussian distributions to the histograms of error estimates, or we can compute the covariance matrix, as follows:

$$\mathrm{cov}(p_i, p_j) = \frac{1}{N-1} \sum_{k=1}^{N} (p_i^k - p_i^n)(p_j^k - p_j^n), \quad (5)$$

where N is the total number of simulations, p_i^n is the nominal value of the ith parameter ($\beta = 1$, $J_{2\odot} = 2.2 \times 10^{-7}$), and p_i^k is the estimated value of the ith parameter from the kth simulation of observations. We used Equation (5) and estimated the formal uncertainties in the solve-for parameters by computing the

square root of diagonal elements. We found

$$\sigma_\beta = 7.4 \times 10^{-4}, \quad (6)$$

$$\sigma_{J_{2\odot}} = 3.7 \times 10^{-8}, \quad (7)$$

with a correlation coefficient of −0.81. These values confirm the covariance analysis results.

5. Conclusions

A modest observing campaign requiring 50–60 hr of Arecibo telescope time over the next five years can provide about 20 range measurements of asteroids whose orbits exhibit large perihelion shift rates. The Arecibo Planetary Radar facility is required for these measurements because its sensitivity is ∼20 times better than that of other radar systems (Naidu et al. 2016), allowing detection of asteroids that are not detectable elsewhere.

The Arecibo measurements will complement existing optical and radar astrometry and enable joint orbital solutions with β and $J_{2\odot}$ as adjustable parameters. Independent, purely dynamical determinations of both parameters are important because they place bounds on theories of gravity and the interior structure the of Sun, respectively.

Our simulation results likely under-estimated actual precision for two reasons. First, we did not attempt to simulate the impact of future optical astrometry nor improvements to the accuracy of star catalogs. Both of these effects will inevitably improve the quality of the orbital determinations. Second, we assumed, based on historical evidence, that radar observers assign fairly conservative uncertainties to their measurements, which often underestimate the precision of the measurements by a factor of ∼3 (Table 2). As a result, we anticipate that the uncertainties of the final estimates will be close to

$$\sigma_\beta \sim 2 \times 10^{-4}, \quad (8)$$

$$\sigma_{J_{2\odot}} \sim 10^{-8}. \quad (9)$$

A.K.V., J.L.M., and A.H.G. were supported in part by the NASA Planetary Astronomy program under grant NNX12AG34G. J.L.M. and A.H.G. were supported in part by NSF Planetary Astronomy program AST-0929830 and AST-1109772. This work was enabled in part by the Mission Operations and Navigation Toolkit Environment (MONTE). MONTE is developed at the Jet Propulsion Laboratory, which is operated by Caltech under contract with NASA.

Software: MONTE v124 (Evans et al. 2016).

ORCID iDs

Ashok K. Verma https://orcid.org/0000-0002-7209-0004
Jean-Luc Margot https://orcid.org/0000-0001-9798-1797
Adam H. Greenberg https://orcid.org/0000-0001-8834-9423

References

Antia, H. M., Chitre, S. M., & Gough, D. O. 2008, A&A, 477, 657
Bertotti, B., Iess, L., & Tortora, P. 2003, Natur, 425, 374
Bierman, G. J. 1977, Factorization Methods for Discrete Sequential Estimation, Vol. 128 (New York: Academic)
Bottke, W. F., Jr., Vokrouhlický, D., Rubincam, D. P., & Nesvorný, D. 2006, AREPS, 34, 157
Evans, S., Taber, W., Drain, T., et al. 2016, presentation at The 6th Int. Conf. on Astrodynamics Tools and Techniques (ICATT), https://indico.esa.int/indico/event/111/session/30/contribution/177/material/paper/0.pdf
Farnocchia, D., Chesley, S. R., Chamberlin, A. B., & Tholen, D. J. 2015, Icar, 245, 94
Farnocchia, D., Chesley, S. R., Vokrouhlický, D., et al. 2013, Icar, 224, 1
Fienga, A., Laskar, J., Kuchynka, P., et al. 2011, CeMDA, 111, 363
Fienga, A., Manche, H., Laskar, J., & Gastineau, M. 2015, CeMDA, 123, 325
Folkner, W. M. 2009, in IAU Symp. 261, Relativity in Fundamental Astronomy: Dynamics, Reference Frames, and Data Analysis, ed. S. A. Klioner, P. K. Seidelmann, & M. H. Soffel (Cambridge: Cambridge Univ. Press), 155
Greenberg, A. H., Margot, J. L., Verma, A. K., et al. 2017, AJ, 153, 108
Kaula, W. M. 2000, Theory of Satellite Geodesy: Applications of Satellites to Geodesy (Mineola, NY: Dover Publications)
Konopliv, A. S., Asmar, S. W., Folkner, W. M., et al. 2011, Icar, 211, 401
Lambert, S. B., & Le Poncin-Lafitte, C. 2009, A&A, 499, 331
Margot, J. L. 2003, AAS Meeting, 34, 06.13
Margot, J. L., & Giorgini, J. D. 2009, in IAU Symp. 261, Relativity in Fundamental Astronomy: Dynamics, Reference Frames, and Data Analysis, ed. S. A. Klioner, P. K. Seidelmann, & M. H. Soffel (Cambridge: Cambridge Univ. Press), 183
Mecheri, R., Abdelatif, T., Irbah, A., Provost, J., & Berthomieu, G. 2004, SoPh, 222, 191
Minor Planet Center. 2017, MPC database, http://www.minorplanetcenter.net/iau/mpc.html
Misner, C. W., Thorne, K. S., & Wheeler, J. A. 1973, Gravitation (San Francisco: Freeman)
Naidu, S. P., Benner, L. A. M., Margot, J. L., Busch, M. W., & Taylor, P. A. 2016, AJ, 152, 99
Nugent, C. R., Margot, J. L., Chesley, S. R., & Vokrouhlický, D. 2012, AJ, 144, 60
Ostro, S. J., & Giorgini, J. D. 2004, in Mitigation of Hazardous Comets and Asteroids, ed. M. Belton et al. (Cambridge: Cambridge Univ. Press), 38
Park, R. S., Folkner, W. M., Konopliv, A. S., et al. 2017, AJ, 153, 121
Pitjeva, E. V., & Pitjev, N. P. 2014, CeMDA, 119, 237
Solomon, S. C., McNutt, R. L., Gold, R. E., et al. 2001, P&SS, 49, 1445
Verma, A. K., Fienga, A., Laskar, J., Manche, H., & Gastineau, M. 2014, A&A, 561, A115
Verma, A. K., & Margot, J. L. 2016, JGRE, 121, 1627
Will, C. M. 2014, LRR, 17, 4